

# Atmospheric Effects and Spectral Vegetation Indices

R. B. Myneni\* and G. Asrar†

*A vegetation/atmosphere radiative transfer method is employed to study atmospheric effects in spectral vegetation indices. A one-dimensional turbid medium model of a vegetation canopy that includes specular reflection and the hot spot effect is used to calculate canopy bidirectional reflectance factors. These are then used to specify the lower boundary condition of the atmospheric radiative transfer problem. A horizontally homogeneous cloudless midlatitude continental atmosphere with both molecular and aerosol loading is assumed throughout. The canopy and atmospheric radiative transfer equations are numerically solved by the discrete ordinates method. A total of 13 discrete wavelengths in the solar spectrum outside the absorption bands of major atmospheric constituents were considered in this study. Spectral and angular distribution of surface radiances above the canopy and atmosphere were evaluated for different solar zenith angles and leaf area indices. The most frequently used spectral vegetation index, NDVI, and variants introduced recently to correct for atmospheric and soil brightness effects (ARVI, SAVI, and SARVI) were calculated to investigate the extent of atmospheric distortion. The nature of the relationship between top-of-the-atmosphere and top-of-the-canopy spectral vegetation indices is studied, and its sensitivity to various problem parameters assessed.*

## INTRODUCTION

Spectral vegetation indices (SVI) are synthesized from spectral reflectance factors using a variety of techniques (Tucker, 1979). A number of SVIs have been proposed

in the literature that employ various combinations (differencing, ratioing, etc.) of vegetation bidirectional reflectance factors (BRFs) at two or more wavelengths. The most common index is the normalized difference vegetation index (NDVI). The component canopy reflectance factors invariably contain contribution from the soil or background litter. A soil-adjusted vegetation index (SAVI) was proposed by Huete (1988) which minimizes soil brightness influences from SVIs involving red and near-infrared wavelengths.

In addition to minimizing the effect of background, top-of-the-atmosphere (TOA) spectral radiance values must be corrected for atmospheric effects to recover the vegetation signal. One such index, the atmospherically resistant vegetation index (ARVI), was recently proposed by Kaufman and Tanré (1992) that incorporates a self-correction process for the atmospheric effect at red wavelength by utilizing the radiance difference between blue and red wavelengths. ARVI can be coupled with SAVI (cf. Kaufman and Tanré, 1992); the resulting index (SARVI) is expected to correct for both atmospheric and background brightness effects.

These indices are related to vegetation parameters of interest such as fractions of absorbed solar and photosynthetically active radiation, canopy photosynthetic and unstressed bulk stomatal conductance efficiencies and land surface albedo (Asrar et al., 1984; Sellers, 1985; Myneni et al., 1992b). This information is needed in all surface energy balance and climate studies (Sellers et al., 1986), productivity analysis (Prince, 1991), and ecosystem models (Peterson and Running, 1989). As a result, these indices form the core of an evolving branch of remote sensing technology with a significant role in the forthcoming Earth Observing System (EOS) era.

Most of the past ground-based analyses were restricted to top-of-the-canopy (TOC) spectral indices. It is of considerable interest to inquire if TOA vegetation indices from remote sensing are similarly related to land surface physical and physiological parameters. Clearly, the question of atmospheric effects has to be addressed.

\* Biospheric Sciences Branch, NASA Goddard Space Flight Center, Greenbelt

† NASA Headquarters, Washington, DC

Address correspondence to R. B. Myneni, Biospheric Sciences Branch, Code 923, NASA / GSFC, Greenbelt, MD 20771.

Received 3 July 1992; revised 7 April 1993.

Moreover, sensitivity of these relationships to problem parameters has also to be assessed. With these considerations in mind, a vegetation / atmosphere radiative transfer method is employed in this study to investigate atmospheric modulation of spectral vegetation indices.

### TOP-OF-THE-CANOPY (TOC) REFLECTANCE FACTORS

Vegetation canopy bidirectional reflectance factors  $R_v$  are evaluated by numerically solving the canopy radiative transfer equation. We assume a horizontally homogeneous vegetation canopy, of finite physical depth, filled densely with small leaves and bounded by a flat Lambertian ground surface. The canopy is illuminated spatially uniformly on top by monodirectional radiation of intensity  $I_v^\dagger$  along  $\Omega'(\mu', \varphi')$ ,  $\mu' < 0$ . The unit vector  $\Omega(\mu, \varphi)$  has an azimuthal angle  $\varphi$  and a polar angle  $\theta = \cos^{-1} \mu$  with respect to the outward normal. The scattered intensity distribution emerging at the top of the canopy in all directions in the upper hemisphere,  $I_v[\Omega(\mu, \varphi)]$ ,  $\mu > 0$ , is the desired solution.

The governing radiative transfer equation and boundary conditions are similar to the ones encountered in atmospheric radiative transfer (next section) with the following important exception (Ross, 1981). The canopy radiative transfer problem is not rotationally invariant, that is, the extinction coefficient depends on the direction of photon travel and the scattering phase function depends on the absolute directions of photon travel  $\Omega'$  and  $\Omega$ . Extinction of radiation in a canopy depends on the leaf area density distribution and leaf normal orientation, and is independent of wavelength. The magnitude of scattered radiation depends strongly on the wavelength of the incident beam. A probabilistic description of the scattering event requires information on the leaf scattering physics in addition to the above two structural parameters. Models of the leaf scattering phase function describing specular reflection at the leaf surface and diffuse scattering in the leaf interior are included in our canopy models (Shultis and Myneni, 1988; Myneni et al., 1990).

A quantitative description of the vegetation-canopy hot-spot effect requires consideration of leaf spatial distribution and size in the transport formulation which leads to correlated probabilities of photon interactions (Myneni et al., 1990). For remote sensing purposes, however, a simple model of the hot spot effect generally suffices. A model for the extinction coefficient that correlates interaction rates between incident and once-scattered photons is used to describe the hot spot effect (Marshak, 1989). Multiple scattering within the canopy and reflection at the soil surface is handled by the standard radiative transfer method. This approach gave results that compared well with measured BRFs of several vegetation canopies (Stewart, 1990). Details on

the problem formulation, solution, benchmarking, and validation can be found in our earlier papers (Myneni et al., 1988a,b; Shultis and Myneni, 1988; Asrar et al., 1989; Stewart, 1990; Myneni et al., 1990; Canapol and Myneni, 1992). The computer code for numerical solution of the canopy radiative transfer equation (RTE) to obtain BRFs ( $R_v$ ) was developed by Stewart (1990) and extensively modified by us recently (Myneni et al., 1992).

### TOP-OF-THE-ATMOSPHERE (TOA) REFLECTANCE FACTORS

Absorption and scattering of radiation in the atmosphere is assumed primarily due to gases and aerosols. Atmospheric optical depth  $\tau_a$ , single scattering albedo  $\omega_a$  and phase function  $P_a$  are parameterized for horizontally homogeneous cloudless atmospheres over midlatitude continental areas (Deepak and Gerber, 1983). Interaction of solar radiation with gaseous molecules is described by Rayleigh scattering. The molecular optical depth  $\tau_a^\dagger$  at wavelength  $\lambda$  in the solar spectrum is evaluated from the refractive index of air and molecular density distribution. Midlatitude summer profiles of temperature and pressure are used to calculate the height distribution of molecular density up to an altitude of 100 km. The Rayleigh phase function  $P^m$  is used to evaluate the scattered photon redistribution in angle. Routines from the 5S code were used to calculate  $\tau_a^\dagger$  and  $P^m$  (Tanré et al., 1990).

The profile of atmospheric aerosol distribution is based on a recommendation by the International Radiation Commission (IRS) applicable to continental areas (Deepak and Gerber, 1983). The report describes aerosol models based primarily on the works of Shettle and Fenn (1979), who developed several aerosol models for a variety of atmospheric conditions with input from many sources. From the various possible aerosol components (e.g., water soluble, dustlike, soot particles, etc.), five aerosol type models were developed assuming external mixing—continental, urban/industrial, maritime, stratospheric, and volcanic models.

The aerosol profile used in our calculations contains a continental tropospheric aerosol distribution in the layer between 0 km and 12 km. The model is composed from 70% dustlike aerosols, 29% water-soluble components, and 1% soot particles. The layer is further divided into a planetary boundary layer contained between 0 km and 2 km, with an aerosol optical depth  $\tau_a^\dagger$  of 0.2 at 0.55  $\mu\text{m}$ . A free tropospheric layer extends from 2 km to 12 km, with  $\tau_{0.55}^\dagger = 0.025$ . The atmospheric layer between 12 km and 30 km is modeled as unperturbed background stratospheric aerosol (75% sulfuric acid droplets) with  $\tau_{0.55}^\dagger = 0.003$ . Likewise, the layer between 30 km and 100 km is modelled as upper atmospheric aerosol, also with 75% sulfuric acid droplets. The total

aerosol optical depth at 0.55  $\mu\text{m}$  in this profile is 0.23. The actual vertical distribution within each of these layers is also given in the IRS report.

The aerosol scattering phase function  $P^a$  is modeled using the Henyey–Greenstein function. Its asymmetry parameter  $g^a$  and the aerosol single scattering albedo  $\omega^a$  are tabulated in the IRS report for several wavelengths in the solar spectrum. These were derived from measured complex indices of refraction and particle size distributions by the application of Mie theory (Deepak and Gerber, 1983). These models, however, do not account for dependence on relative humidity (RH). Thus, our results are valid for atmospheric conditions under 75% RH. Assuming external mixing (Tanré et al., 1983), the total atmospheric optical depth  $\tau_a$ , single scattering albedo  $\omega_a$ , and the scattering phase function  $P_a$  were evaluated, that is,

$$\begin{aligned}\tau_a &= \tau^m + \tau^a, \\ \omega_a &= \tau^m / \tau_a + \omega^a \tau^a / \tau_a, \\ P_a &= P^m \tau^m / \tau_a + P^a \tau^a / \tau_a.\end{aligned}\quad (1)$$

Thirteen wavelengths in the solar spectrum were considered in this study, viz., 0.4  $\mu\text{m}$ , 0.488  $\mu\text{m}$ , 0.515  $\mu\text{m}$ , 0.55  $\mu\text{m}$ , 0.633  $\mu\text{m}$ , 0.694  $\mu\text{m}$ , 0.860  $\mu\text{m}$ , 1.06  $\mu\text{m}$ , 1.3  $\mu\text{m}$ , 1.536  $\mu\text{m}$ , 1.8  $\mu\text{m}$ , 2.0  $\mu\text{m}$ , and 2.25  $\mu\text{m}$ . Leaf hemispherical reflectance and transmittance at these wavelengths were calculated by digitizing the spectra measured by Hall for several vegetation species (F. G. Hall, personal communication). Measured hemispherical reflectance of three soil types (bright, dark, and very dark) were obtained from Irons et al. (1989).

We now focus our attention on the radiative transfer problem. Consider a horizontally homogeneous atmosphere of finite optical depth  $\tau_a$ , illuminated spatially uniformly on top ( $\tau = 0$ ) and bound at the bottom ( $\tau = \tau_a$ ) by a vegetation canopy. Assuming no polarization, frequency shifting interactions, and emission, the steady state monochromatic radiance or intensity distribution function  $I(\tau, \Omega)$  is given by the radiative transfer equation in plane geometry

$$-\mu \frac{\partial}{\partial \tau} I(\tau, \Omega) + I(\tau, \Omega) = \frac{\omega_a}{4\pi} \int_{4\pi} d\Omega' P_a(\Omega' \rightarrow \Omega) I(\tau, \Omega'), \quad (2)$$

where  $\omega_a$  is the single scattering albedo and  $P_a$  is the scattering phase function for photon scattering from the direction  $\Omega'$  into  $\Omega$ . Again, the unit vector  $\Omega(\mu, \varphi)$  has an azimuthal angle  $\varphi$  and a polar angle  $\theta = \cos^{-1} \mu$  with respect to the outward normal (opposite to the  $\tau$ -axis, which is directed down into the atmosphere); consequently,  $\mu \in (0, 1)$  denotes upward directions of photon travel and vice versa.

The atmosphere is illuminated from above by parallel beams of monodirectional solar radiation of intensity  $I_0$  incident along  $\Omega_0(\mu_0 < 0)$ ,

$$I(\tau = 0, \Omega) = I_0 \delta(\Omega - \Omega_0), \quad \mu < 0. \quad (3)$$

At the bottom of the atmosphere, a horizontally homogeneous, absorbing and scattering vegetation canopy reflects radiation back into the atmosphere according to

$$\begin{aligned}I(\tau = \tau_a, \Omega) &= \frac{1}{\pi} \int_{2\pi} d\Omega' R_v(\Omega' \rightarrow \Omega) \\ &\times |\mu'| I(\tau_a, \Omega'), \quad \mu' < 0, \mu > 0,\end{aligned}\quad (4)$$

where  $R_v$  is the canopy bidirectional reflectance factor (BRF) defined as

$$R_v(\Omega' \rightarrow \Omega) = \frac{\pi I_v(\tau_a, \Omega)}{|\mu'| I_i(\tau_a, \Omega')}, \quad \mu' < 0, \mu > 0. \quad (5)$$

In Eq. (5),  $I_i$  is the intensity incident on the canopy along  $\Omega'$  and  $I_v$  is the canopy radiance along  $\Omega$  obtained as a solution of the canopy RTE. Solution of the atmospheric RTE [Eq. (2)] subject to the boundary conditions [Eqs. (3) and (4)] gives the top-of-the-atmosphere radiance field [ $I(\tau = 0, \Omega), \mu > 0$ ].

## NUMERICAL SOLUTION METHODS

The standard discrete ordinates method is employed to solve the atmospheric and vegetation canopy radiative transfer equations. In this method, photons are allowed to travel in a finite (144) number of directions in the unit sphere. These directions are chosen such that their direction cosines serve as ordinates of the quadrature schemes that replace the integral member in the transfer equation [rhs of Eq. (2)]. Thus, the scattering phase function is replaced by a matrix of cross section values that define scattering between the discrete directions, which conveniently alleviates the nonrotational invariance of the canopy transport equation. The spatial derivative in Eq. (2) is replaced by a first-order finite difference scheme to result in a linear system of algebraic equations that is solved by iteration on the scattering source. Acceleration of this iteration is accomplished by any one of the standard techniques such as the coarse mesh rebalancing method. The particular discrete ordinates method used in this study was rigorously benchmarked and found to be four-digit accurate (Myneni et al., 1988a; Ganapol and Myneni, 1992). The method was also validated with experimental data of reflectance spectra collected over maize and soybean (Myneni et al., 1988b; Shultis and Myneni, 1988), prairie grassland (Asrar et al., 1989) and forest canopies (Myneni et al., 1992a).

For a given incident direction  $\Omega'$ , the vegetation canopy BRFs are calculated, by numerically solving the canopy RTE, for all the 72 directions  $\Omega$  in the upper hemisphere,  $R_v(\Omega' \rightarrow \Omega)$ . This procedure is repeated for all the 72 directions in the downward hemisphere of the unit sphere. The resulting matrix  $R_v$  is then used in the lower boundary condition of the atmospheric RTE

[Eq. (4)]. The atmospheric RTE is numerically solved, again by the discrete ordinates method, to evaluate the radiance distribution at the top of the atmosphere. We implemented interpolation schemes that allow decoupling the quadrature orders between the canopy and atmospheric radiative transfer calculations. This allows the boundary condition for the atmospheric RTE to be specified in a finer grid without the attendant calculations. Essentially this involves performing one additional sweep of the spatial grid, using converged source distribution, into the desired angular grid. This entire scheme is wavelength specific and a detailed energy balance is performed both at the canopy and atmospheric level. Typical CPU time for a one-wavelength calculation of the vegetation/atmosphere BRFs is about 2 h on a Sparcstation 2 (note that the canopy RTE is solved 72 times and the atmospheric RTE once).

## RESULTS AND DISCUSSION

### Angular and Spectral Distributions

The angular distribution of top-of-the-canopy (TOC) and top-of-the-atmosphere (TOA) radiance in the solar principal plane at red and near-infrared wavelengths is shown in Figures 1a and 1b. Atmospheric path radiance, comprising of photons scattered in the atmosphere only, is shown in Figure 1c. The canopy leaf area index is 3 and an uniform leaf normal orientation distribution is assumed. The results are for two solar zenith angles ( $\theta_0 = 15^\circ$  and  $60^\circ$ ).

Angular distributions above the canopy are anisotropic with the distinctive hot spot in the retro-solar direction, at both wavelengths (Fig. 1a). The hot spot radiance is, in general, the maximum of the distribution. The minimum is found about the nadir on the forward scattering side. The degree of anisotropy increases with solar zenith angle. The hot spot effect is more pronounced in the red than near-infrared because of the contrast between sunlit and shaded elements. These features agree well with experimental data (Deering, 1989; Myneni et al., 1992c). Vegetation canopies are strong backscatterers because the characteristic dimension of the scatterers (leaves) is much larger than the wavelength of the incident beam.

Radiances above the atmosphere differ from those above the canopy both in terms of their magnitude and angular distribution (Fig. 1b). The net atmospheric effect, which is the difference between TOA and TOC values, decreases almost linearly with increasing surface reflectance (Kaufman, 1989). It is positive at shorter wavelengths (viz., red), where atmospheric scattering plays a dominant role and negative at longer wavelengths (near-infrared), where aerosol and gaseous absorption predominate. For instance, TOA radiance at the red wavelength is 2–10 times greater than TOC red radiance, depending upon the view and solar zenith

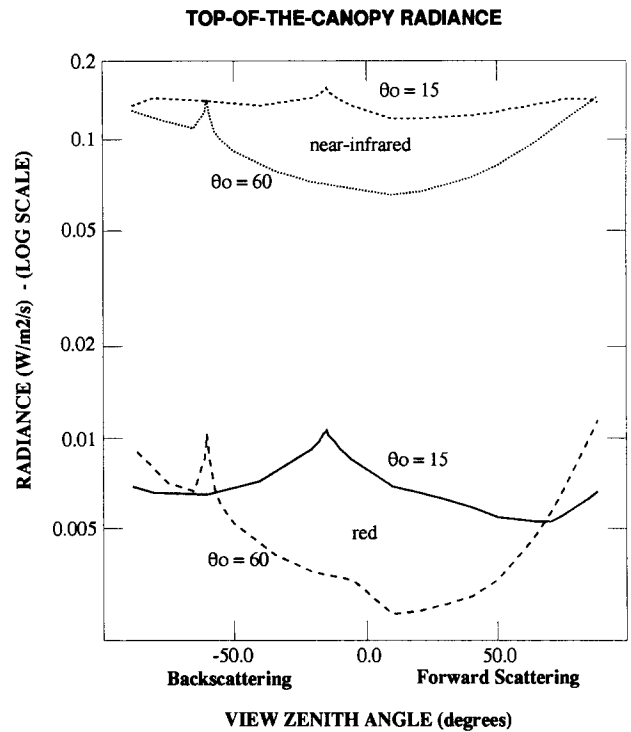
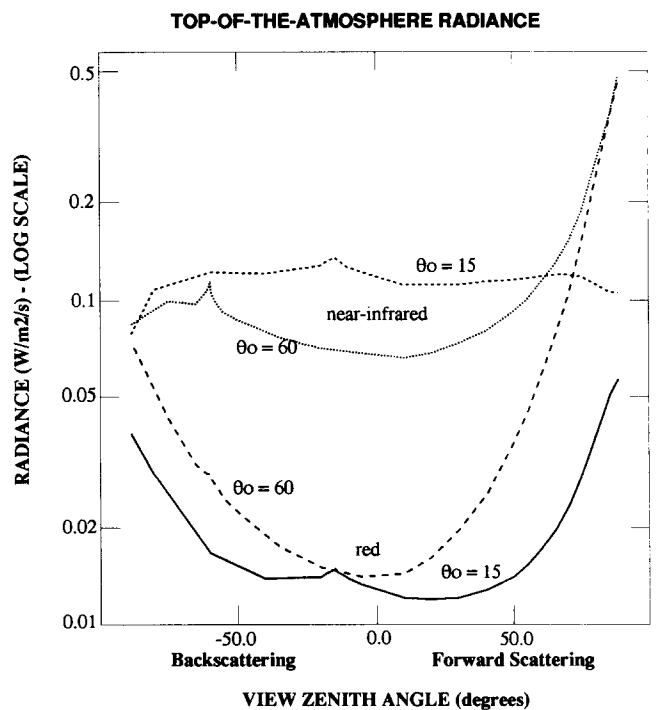


Figure 1a. Angular distribution of top-of-the-canopy radiance in the solar principal plane at red and near-infrared wavelength. Unit incident irradiance is assumed such that radiance  $\times \pi$  is the corresponding bidirectional reflectance factor.  $\theta_0$  is the solar zenith angle in degrees.

Figure 1b. Angular distribution of top-of-the-atmosphere radiance in the solar principal plane at red and near-infrared wavelength. Unit incident irradiance is assumed such that radiance  $\times \pi$  is the corresponding bidirectional reflectance factor.  $\theta_0$  is the solar zenith angle in degrees.



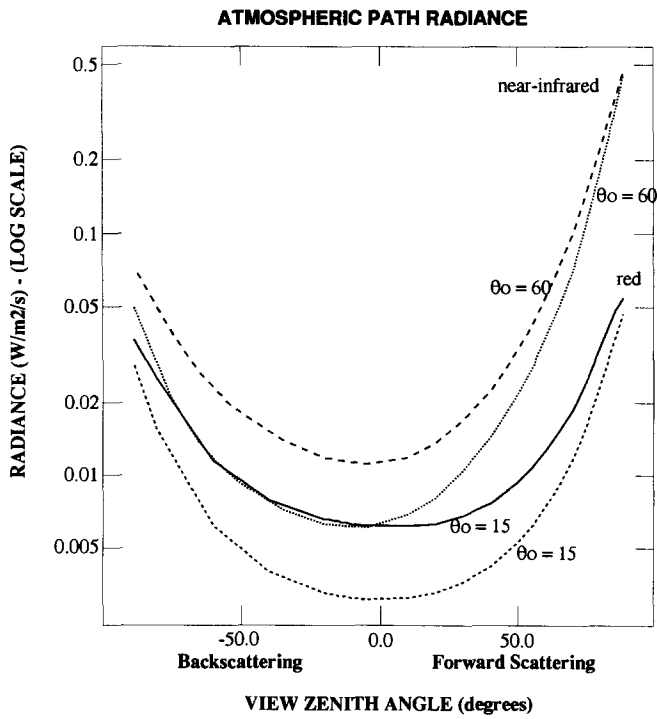


Figure 1c. Angular distribution of atmospheric path radiance in the solar principal plane at red and near-infrared wavelength.  $\theta_0$  is the solar zenith angle in degrees.

angles. The hot spot effect so distinctive at this wavelength in TOC radiance distribution is masked due to scattering in the atmosphere. Absorption in the atmosphere and surface scattering increases with wavelength from  $\approx 0.7 \mu\text{m}$  onwards. At near-infrared wavelengths, the net atmospheric effects is slightly negative. Thus, TOA radiance distribution is similar to that above the canopy.

The anisotropy of TOA radiance distribution increases dramatically with solar zenith angle. Atmospheric effects are most pronounced at oblique look angles, especially in the forward scattering directions irrespective of wavelength. Angular atmospheric effects are best understood from angular distribution of path radiance (Fig. 1c). Path radiance at nadir view direction varies only slightly with solar zenith angle, but increases sharply at oblique view angles, especially in the forward scattering directions. Therefore, view directions about the nadir are least affected by the atmospheric effects, and TOA radiance distribution corresponds closely with TOC radiance distribution. The range of this interval decreases with solar zenith angle, and outside this range the path radiance masks the signal from the canopy.

Reflectance spectra in the range  $0.4\text{--}2.25 \mu\text{m}$  observed above the canopy and atmosphere for a solar zenith angle of  $30^\circ$ , and five view zenith angles in the solar principal plane are shown in Figures 2a and 2b. The distortion of the canopy reflectance spectrum due

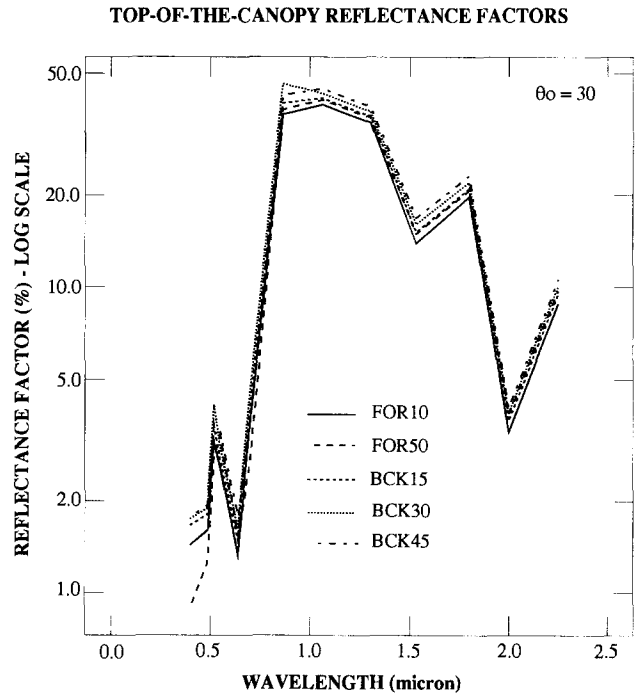


Figure 2a. Top-of-the-canopy reflectance spectra in the  $0.4\text{--}2.25 \mu\text{m}$  range for a solar zenith angle of  $30^\circ$  at five view zenith angles in the solar principal plane.

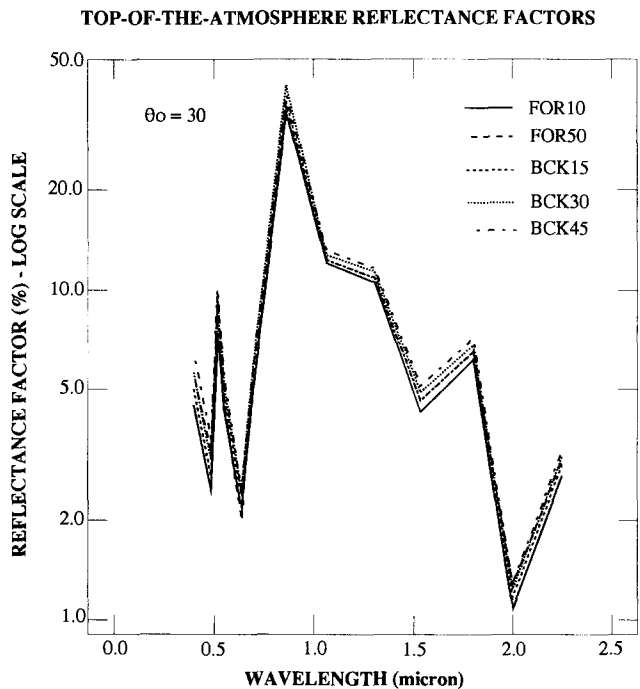


Figure 2b. Top-of-the-atmosphere reflectance spectra in the  $0.4\text{--}2.25 \mu\text{m}$  range for a solar zenith angle of  $30^\circ$  at five view zenith angles in the solar principal plane.

to scattering and absorption in the atmosphere can be clearly seen in these figures. At the shorter wavelengths ( $< 0.7 \mu\text{m}$ ), the atmospheric effect is positive due to strong molecular scattering. Conversely, at the longer

wavelengths ( $>1.0 \mu\text{m}$ ) absorption in the atmosphere damps the vegetation signal resulting in a negative atmospheric effect. The minimum reflectance factor shifts from a view zenith angle of  $50^\circ$  in the forward scattering directions at visible wavelengths to a view zenith angle of  $10^\circ$  at near- and mid-infrared wavelengths (Fig. 2a). Similarly, the maximum value shifts from the retrosolar direction at  $\approx 1.0 \mu\text{m}$  to a view zenith of  $45^\circ$  in the backscattering hemisphere. In the case of TOA reflectance factors, the minimum is about the nadir at all wavelengths (Fig. 2b). These differences are in general quite small. It appears from these results that the reflectance spectra contain valuable information for correcting atmospheric effects, a feature exploited in the derivation of ARVI (next section). Also, data from high spectral resolution spectroradiometers can be utilized to estimate canopy parameters, snow cover, integrated atmospheric water vapor, etc., during the EOS era.

### Spectral Vegetation Indices

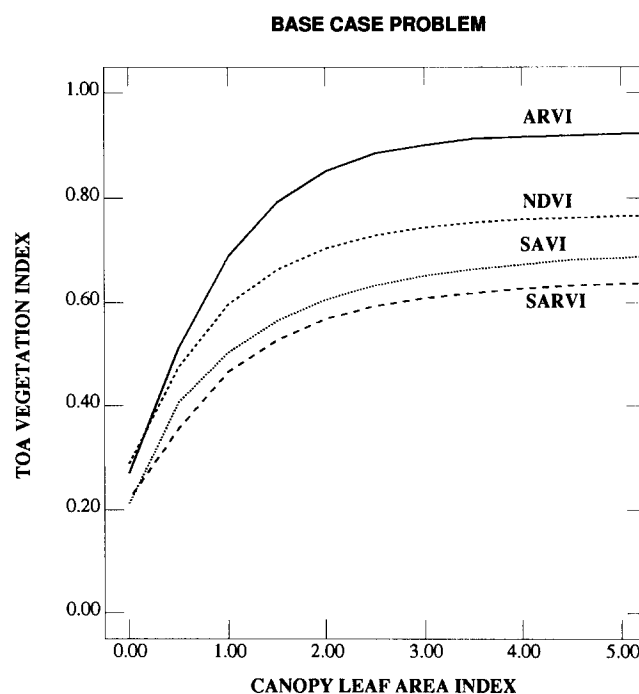
A number of spectral vegetation indices (SVIs) have been proposed in the literature that employ various combinations (differencing, ratioing, etc.) of vegetation BRFs at two or more wavelengths. The most common index is the normalized difference vegetation index (NDVI), evaluated as the contrast in canopy reflectance at near-infrared and red wavelengths, normalized to their sum. The component canopy reflectance factors invariably contain contribution from the soil or background. Consequently, the relationship between SVI and a canopy parameter of interest in remote sensing (e.g., fraction of absorbed photosynthetically active radiation) is sensitive to background reflectance (e.g., Choudhury, 1987). A soil-adjusted vegetation index (SAVI) was proposed by Huete (1988) which minimizes soil brightness influences in spectral vegetation indices involving red and near-infrared wavelengths.

In addition to minimizing background brightness effects, TOA spectral radiance values must be corrected for atmospheric effects to recover the vegetation signal. Recently, an atmospherically resistant vegetation index (ARVI) was proposed by Kaufman and Tanré (1992) that incorporates a self-correction process for atmospheric effects at the red wavelength. Specifically, the difference in the TOA radiance between the blue ( $0.47 \mu\text{m}$ ) and red ( $0.6\text{--}0.7 \mu\text{m}$ ) wavelengths is used to correct for the atmospheric effect at the red wavelength. They report that ARVI is four times less sensitive to atmospheric effects than NDVI based on numerical investigations with the 5S code. ARVI can be coupled with SAVI (cf. Kaufman and Tanré, 1992); the resulting index (SARVI) is expected to correct for both atmospheric effects and background brightness, but no results were presented in their article. In this and the following section, we perform a comparative analysis of the four indices and their sensitivity to the various problem parameters.

A base case set of problem parameters is defined to facilitate the following analysis. The leaf normal orientation is assumed uniform. A bright (reflective) soil background is assumed and reflectance values digitized from curves published by Irons et al. (1989) were utilized. The solar zenith angle is  $30^\circ$  and a horizontally homogeneous cloudless midlatitude continental atmosphere is used to calculate TOA radiances. The relationship between spectral vegetation indices evaluated from TOA radiances and canopy leaf area index (LAI) is shown in Figure 3. NDVI and SAVI approach an asymptotic value at  $\text{LAI} < 2$ . Their dynamic range is also small as compared to either ARVI or SARVI. ARVI is about 50% greater than NDVI for dense canopies ( $\text{LAIs} > 4\text{--}5$ ). Both NDVI and SAVI are susceptible to atmospheric effects because of the large positive net atmospheric effect at the red wavelength. Hence, the contrast between near-infrared and red reflectance is reduced in TOA radiances. ARVI corrects for the atmospheric effect in the red by using TOA radiance difference between blue and red wavelengths, thereby increasing the contrast. This suggests that ARVI is preferable in vegetation remote sensing because of its atmospheric correction properties and consequent sensitivity to LAI.

The angular distribution of NDVI and ARVI in the solar principal plane for the base case problem is shown in Figure 4. Sparse ( $\text{LAI} = 0.5$ ) and dense canopy ( $\text{LAI} = 5$ ) results are shown to assess the interaction between canopy and soil contributions. NDVIs evaluated from TOC and TOA radiances are also shown in

Figure 3. Top-of-the-atmosphere (TOA) spectral vegetation indices vs. vegetation canopy leaf area index in the base case.



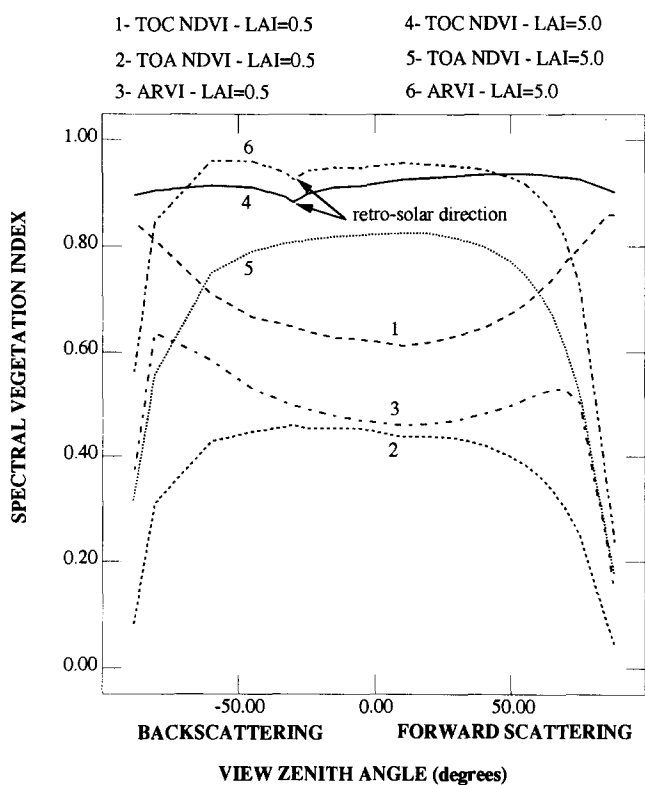


Figure 4. Angular distributions of NDVI and ARVI in the solar principal plane for the base case problem.

this figure together with ARVI (evaluated from TOA radiance field) to characterize effects in NDVI. The dense vegetation TOC NDVI angular distribution (curve 4) shows that the minimum value of NDVI in the principal plane is along the retrosolar direction. The hot spot effect in this direction results in a high red canopy reflectance which decreases the contrast (lower NDVI). Also, NDVIs in the backscattering directions are lower than those in the forward scattering directions—due to strong backscattering that is characteristic of all vegetation canopies. The ratio of backscattering to forward scattering is higher at red than at near-infrared wavelength. This behavior is also seen in the First International Field Experiment (FIFE) experimental data set (Ahmad and Deering, 1992).

The dense vegetation TOA NDVI angular distribution in the principal plane (curve 5) clearly shows the nature of the atmospheric effect. TOA NDVI is always smaller than TOC NDVI because of the positive net atmospheric effect at the red wavelength. The atmospheric effect increases dramatically because of steep increase in atmospheric path radiance for view zenith angles greater than  $60^\circ$ , both in the forward and backscattering directions (Figs. 1b and 1c). The dense canopy ARVI distribution in the principal plane (curve 6) is remarkably similar to TOC NDVI distribution (curve 4) for moderate view zenith angles ( $< 50^\circ$ ). The minimum due to the hot spot effect is apparent in ARVI, indicating

that, within this view angle range, atmospheric effects have been corrected.

The above discussion is limited to the case of a dense vegetation canopy, where soil contribution in TOC and TOA radiance field is usually negligible. The TOC NDVI angular distribution in the principal plane for sparse canopies (curve 1) shows that it is symmetric about the nadir where the minimum value is encountered. This distribution follows from the assumption that the soil is a Lambertian scatterer. The TOA NDVI distribution for a sparse canopy (curve 2) is similar to that of a dense canopy (curve 5), but smaller in magnitude, indicating that TOA NDVI angular distribution is more or less dictated by the angular distribution of path radiance. If correction for this distortion is applied, as in the case of ARVI, the original TOC distribution is recovered for most of the view directions of practical interest (curve 3 versus curve 1, for instance). The original TOC magnitude is not recovered, however, 1) because of the residual atmospheric effect (viz., the net negative atmospheric effect at near-infrared) and 2) because the difference between blue and red reflectance for bare soils is larger than for dense vegetation. This introduces a nonnegligible spurious atmospheric effect that is not present in NDVI. It should be pointed out that NDVI and ARVI are not numerically equivalent but are linearly related (Kaufman and Tanré, 1992).

#### Sensitivity to Problem Parameters

It is of interest to investigate the relationship between TOC and TOA spectral vegetation indices and how this relationship is influenced by variation in problem parameters. The base case problem parameter set defined previously was used to accomplish this. Fifteen vegetation canopies were simulated with leaf area index ranging from 0.5 to 10. Sensitivity analysis was performed by varying one problem parameter at a time. The five problem parameters for which sensitivity was analyzed are 1) leaf normal orientation, 2) leaf optical properties at visible wavelengths, 3) soil reflectance, 4) solar zenith angle, and 5) aerosol optical depth. In all cases nadir bidirectional reflectance factors were used to evaluate various spectral indices.

The influence of leaf normal orientation distribution on the relationship between TOA and TOC vegetation indices is shown in Figures 5a and 5b. Planophile and erectophile leaf normal distributions were utilized because they represent extreme cases of mostly horizontal and mostly vertical leaf orientations, respectively. The slope of the relationship between TOA NDVI and TOC NDVI is less than unity ( $\approx 0.82\text{--}0.85$ ), indicating a reduction in contrast between near-infrared and red reflectance due to a positive net atmospheric effect at the red wavelength. Leaf normal orientation does not appear to influence this relationship. Similar observations can

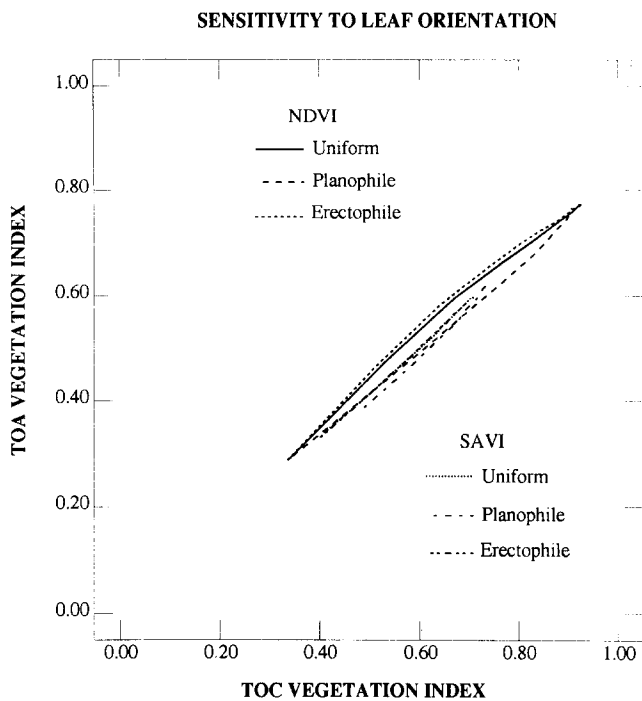


Figure 5a. Influence of leaf normal orientation distribution on the relationship between top-of-the-atmosphere (TOA) and top-of-the-canopy (TOC) spectral vegetation indices.

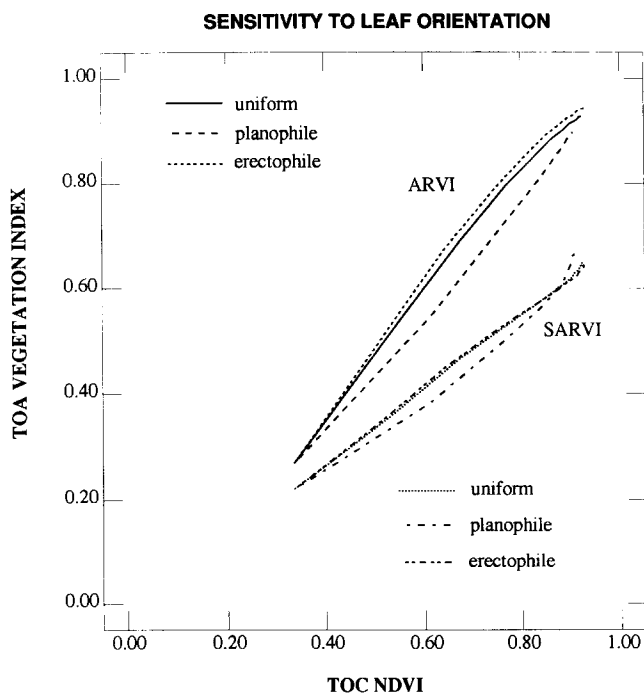


Figure 5b. Influence of leaf normal orientation distribution on the relationship between top-of-the-atmosphere (TOA) vegetation indices, ARVI and SARVI, to top-of-the-canopy (TOC) NDVI.

be made about the relationship between TOA SAVI and TOC SAVI.

The slope of the relationship between ARVI and TOC NDVI is close to unity, indicating that atmospheric

effects have been corrected. This relationship is also nearly invariant of the canopy leaf normal orientation distribution. This is an important result because TOC NDVI has been shown to be related to fraction of solar and photosynthetically active radiation absorbed by the canopy and its photosynthetic and bulk stomatal conductance efficiencies (Asrar et al., 1984; Sellers, 1985; Goward and Huemmerich, 1992; Myneni et al., 1992b,c). The relationship between SARVI and TOC NDVI is similarly almost independent of leaf normal orientation distribution but the slope is less than unity ( $\approx 0.7$ ) because NDVI is sensitive to soil brightness (Fig. 7a), while SARVI corrects for soil influences to a certain extent (Fig. 7b).

The reflectance spectrum of a vegetation canopy exhibits a characteristic shape (Fig. 2a), and, in the TOA radiance field, atmospheric influences are imposed on the canopy spectral signal (Fig. 2b). The effective leaf optical properties are sensor-dependent because they are reported as integral values over the bandwidth of a specific sensor. Thus, a question arises as to the comparability of data collected with different sensors. For instance, one could enquire how TOA vegetation indices evaluated from radiance fields measured by sensors of different bandwidths differ. A sensitivity analysis was performed with leaf optical properties (leaf hemispherical reflectance and transmittance) in the visible region of the solar spectrum doubled and halved. The resulting relationships between TOA and TOC indices are shown in Figures 6a and 6b. It is apparent that variations in leaf optical properties do not appreciably alter the relationship between TOA and TOC vegetation indices, although the index SAVI is generally more sensitive. Thus, a multisensor data set may be used to chart temporal profiles of canopy spectral vegetation indices. An important assumption here is that the footprint and filter functions of the sensors are comparable.

The radiance field above the canopy and atmosphere contains contributions from the background soil surface. The influence of soil reflectance decreases as canopy leaf area increases, and, for sufficiently dense canopies ( $LAI > 7$ ), the effect of reflection at the soil may be ignored. NDVI of a bare soil can range between 0.08 and 0.33 (Stoner and Baumgardner, 1981). Like atmospheric effects, soil effects perturb the vegetation spectra and corrections must be applied to recover the information content of the vegetation signal. For this purpose, a sensitivity analysis was performed with three soil types of varying brightness (Irons et al., 1989). The resulting relationships between TOA and TOC vegetation indices are shown in Figures 7a and 7b.

The relationship between TOA and TOC NDVI is nearly dependent on the soil type. The slope of this relationship decreases with soil brightness (Fig. 7a). The difference between the three relationships is pronounced in case of sparse canopies (low NDVIs) because of the dominance of soil contribution to the surface

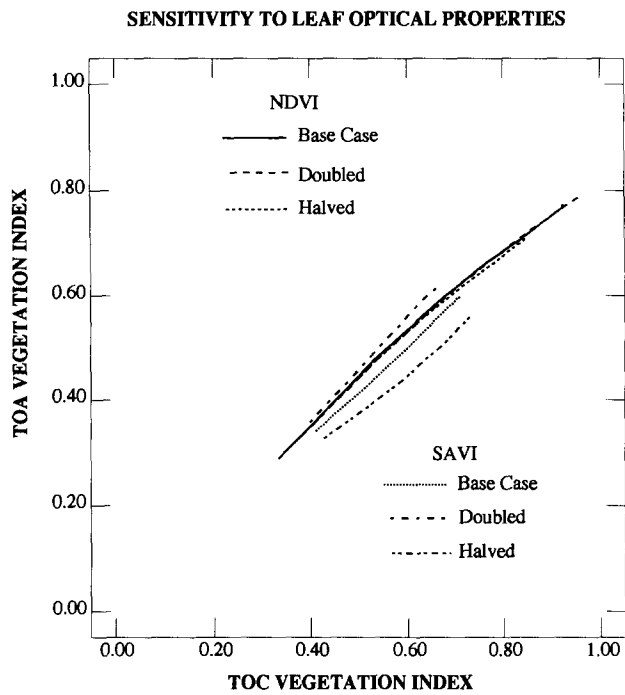


Figure 6a. Influence of leaf optical properties at visible wavelengths on the relationship between top-of-the-atmosphere and top-of-the-canopy spectral vegetation indices. Leaf optical properties in the base case problem parameter set were doubled and halved to effect a sensitivity analysis.

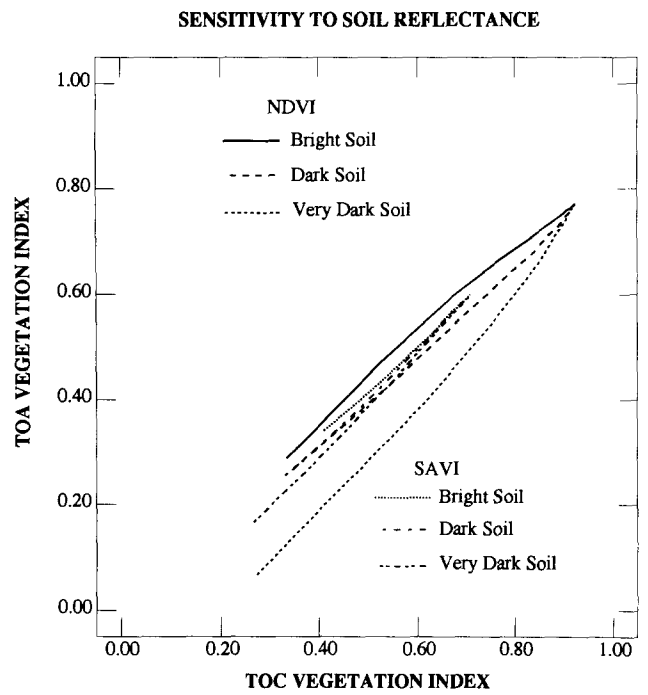


Figure 7a. Influence of soil brightness on the relationship between top-of-the-atmosphere (TOA) and top-of-the-canopy (TOC) spectral vegetation indices.

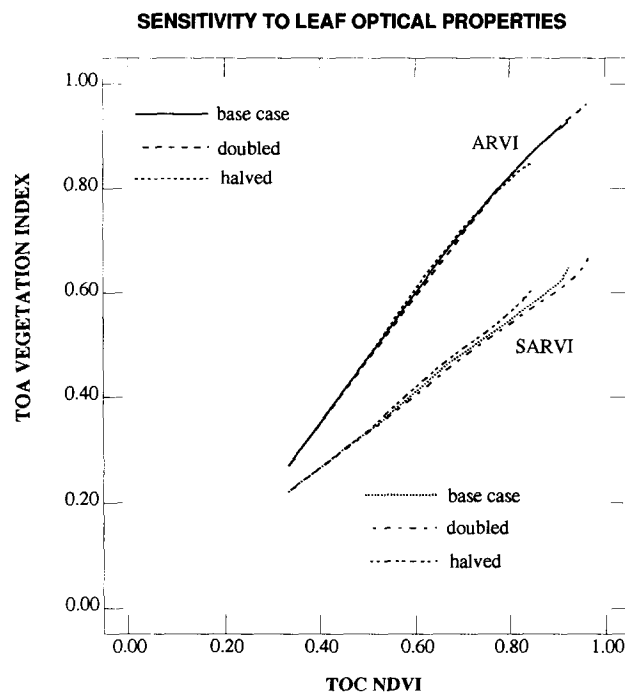


Figure 6b. Influence of leaf optical properties at visible wavelengths on the relationship between AVRVI and SARVI to top-of-the-canopy NDVI. Leaf optical properties in the base case problem parameter set were doubled and halved to effect a sensitivity analysis.

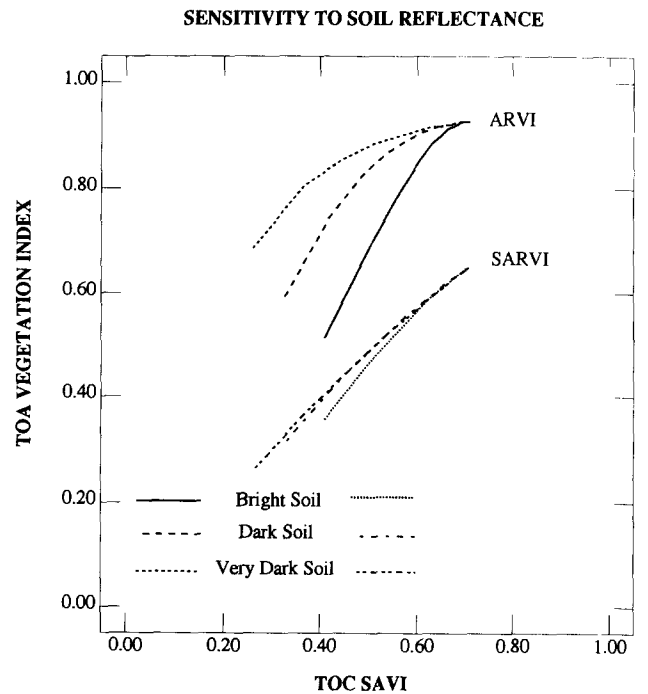


Figure 7b. Influence of soil brightness on the relationship between top-of-the-atmosphere (TOA) vegetation indices, ARVI and SARVI, to top-of-the-canopy (TOC) SAVI.

radiance field. Soil effects generally decrease with increasing leaf area (higher NDVIs), and it can be seen from Figure 7a that the curves converge for dense canopies. On the other hand, the relationship between

TOA and TOC SAVI is independent of soil brightness (Fig. 7a). However, this idea does not mean that atmospheric effects were corrected as can be evidenced from the slope of the relationship (also see Fig. 8a).

The relationship between ARVI and TOC SAVI is shown in Figure 7b for three different soil brightnesses. TOC SAVI was chosen in this particular case because it is independent of soil brightness and is a true measure of the canopy reflectance contrast between near-infrared and red wavelengths. An index such as ARVI that corrects for atmospheric effects (Fig. 5b) is still subject to soil brightness effects because of its close correspondence to TOC NDVI (Fig. 7b). The spectral index SARVI which incorporates corrections for both atmospheric and soil effects is more tightly coupled to TOC SAVI (Fig. 7b).

It should be pointed out that the coefficient  $L$  used in evaluating SAVI and SARVI is a function of the leaf area index of the canopy (and presumably dependent on other canopy problem parameters). A constant value of 0.5 was used in this analysis as recommended by Huete (1988). As pointed out by Kaufman and Tanré (1992), it is not clear if the same value of  $L$  is valid for evaluating SARVI. A rigorous physical formulation based on radiative transfer for decoupling soil and vegetation contributions in the surface radiance field is desirable and will be the subject of a future investigation.

The influence of variations in solar zenith angle  $\theta_0$  on the relationship between TOA and TOC spectral indices is shown in Figures 8a and 8b. The relationship between TOA NDVI and TOC NDVI shows a small variation within the solar zenith range 5–30°. However, for a high solar zenith angle the relationship is dramatically altered, and the slope decreases from 0.85 ( $\theta_0 = 5\text{--}30^\circ$ ) to 0.55 ( $\theta_0 = 60^\circ$ ). TOA near-infrared radiance about the nadir decreases due to the increased atmospheric absorption with increasing solar zenith angle (Fig. 1b), while, at the red wavelength, higher solar zenith angles result in increased atmospheric scattering (Fig. 1b). Although atmospheric path radiance increases with increasing solar zenith angle irrespective of wavelength, large changes are observed only in oblique view directions ( $> 60^\circ$ ) (Fig. 1c). Consequently, the increased net atmospheric effect (positive at red and negative at near-infrared) results in a markedly decreased contrast (TOA NDVI) along near-nadir view directions (Fig. 8a). Similar remarks can be made about the relationship between TOA SAVI and TOC SAVI.

The relationship between ARVI and TOC NDVI is independent of the solar zenith angle within the range 5–60° as can be seen from Figure 8b, and the slope of this relationship is close to unity. This indicates that the larger net atmospheric effect encountered at high solar zenith angles are completely corrected by ARVI, and to a lesser extent by SARVI. It should be noted that the value of  $\gamma$  in ARVI (Kaufman and Tanré, 1992)

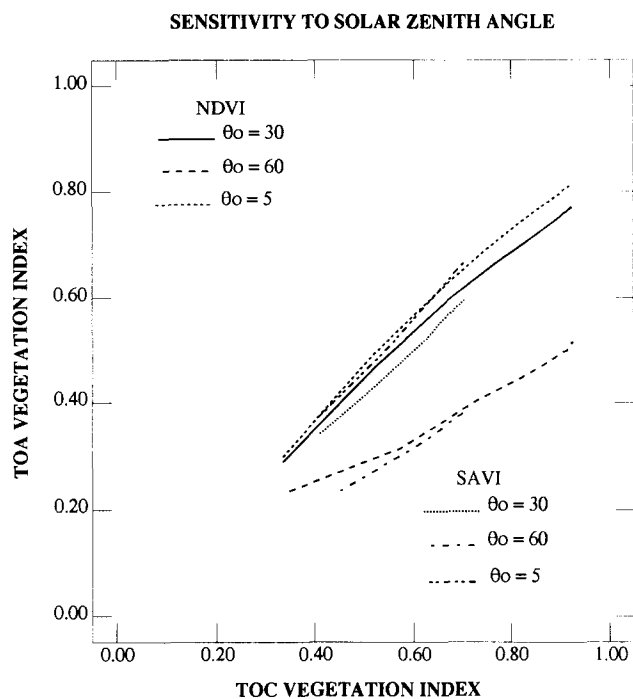


Figure 8a. Influence of solar zenith angle  $\theta_0$  on the relationship between top-of-the-atmosphere (TOA) and top-of-the-canopy (TOC) spectral vegetation indices.

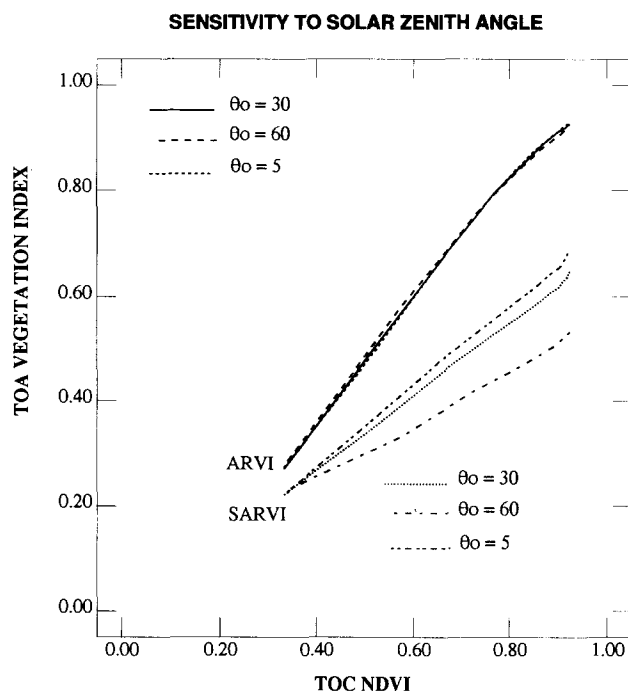


Figure 8b. Influence of solar zenith angle  $\theta_0$  on the relationship between top-of-the-atmosphere (TOA) vegetation indices, ARVI and SARVI, to top-of-the-canopy (TOC) NDVI.

was evaluated for each solar zenith angle ( $\theta_0 = 5$ ,  $\gamma = 0.75$ ;  $\theta_0 = 30$ ,  $\gamma = 0.82$ ; and  $\theta_0 = 60$ ,  $\gamma = 1.1$ ). This particular result has a definite practical value, if one considers that most remote measurements are made at differ-

ent sun positions for logistical reasons (satellite overpass frequency, cloud cover, etc.). For instance, the observation time for the Landsat multispectral scanner (MSS) is 0930 h, for NOAA-8 Advanced Very High Resolution Radiometer (AVHRR) 0730 h, and for NOAA-9 AVHRR 1430 h. Associated with these differences in the time of observation, there is also a seasonal variation of solar zenith angle. For observations by geostationary satellites like GOES and METEOSAT, the solar angle varies throughout the day. Thus, the atmospheric correction inherent in ARVI is an important result of practical value. The index SARVI, on the other hand, still exhibits sensitivity to solar zenith angle changes implying a loss of ability to correct for atmospheric effects (Fig. 8b).

The influence of variations in aerosol optical depth on the relationship between TOA and TOC vegetation indices is shown in Figures 9a and 9b. Aerosol optical depth in the base case corresponds to a continental aerosol profile (third section), and, to assess its sensitivity, these values were doubled (turbid atmosphere) and halved (clear atmosphere). Rayleigh scattering is included in all the three cases by specifying a midlatitude summer profile of molecular density distribution. The slope of the relationship between TOA NDVI and TOC NDVI decreases from  $\approx 0.85$  to  $\approx 0.75$  when the aerosol optical depth is doubled. This can also be intuitively expected—increasing aerosol optical depth decreases the contrast between near-infrared and red reflectance and vice versa. In the ideal case of a very clear atmosphere the slope of the relationship between TOA and TOC spectral indices is close to unity (a trend that can be seen in Fig. 9a).

Interestingly, when aerosol optical depth is doubled, the slope of the relationship between ARVI and TOC NDVI decreases from  $\approx 1.0$  to  $\approx 0.9$ , indicating that a certain amount of atmospheric effect still persists. This is in spite of the case-specific  $\gamma$  values used in the evaluation of ARVI ( $\gamma = 0.82, 0.73,$  and  $0.47$  in the base, doubled, and halved scenarios). ARVI corrects for the positive net atmospheric at the red wavelength but not for the net negative atmospheric effect at the near-infrared wavelength. Obviously, the latter increases with aerosol optical depth to an extent that merits full consideration. In any case, one should be aware of residual atmospheric effects in ARVI, especially under turbid atmospheric conditions.

## SUMMARY AND CONCLUSIONS

A vegetation/atmosphere radiative transfer method is employed to study atmospheric effects in spectral vegetation indices. A one-dimensional turbid medium model of a vegetation canopy that includes specular reflection and the hot spot effect is used to calculate canopy bidirectional reflectance factors. These are then used to specify the lower boundary condition of the atmospheric

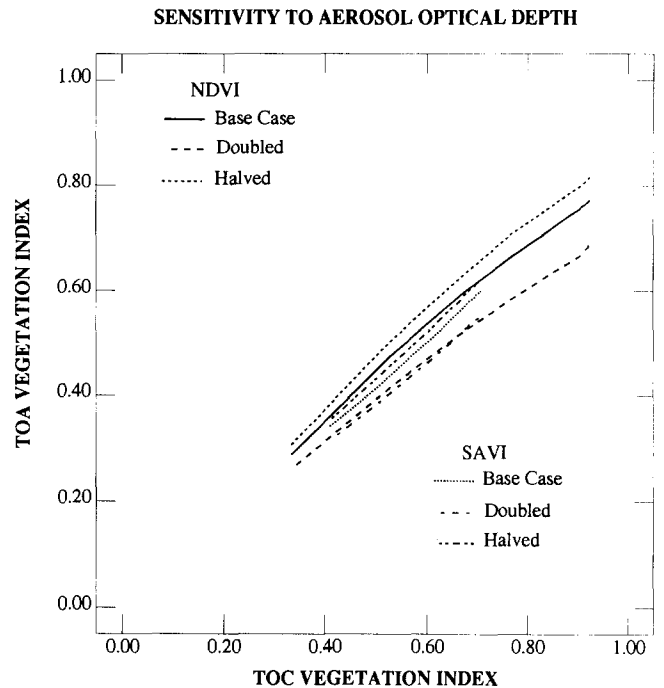


Figure 9a. Influence of aerosol optical depth on the relationship between top-of-the-atmosphere and top-of-the-canopy spectral vegetation indices. Aerosol optical depth in the base case problem parameter set was doubled (turbid atmosphere) and halved (clear atmosphere) to effect a sensitivity analysis.

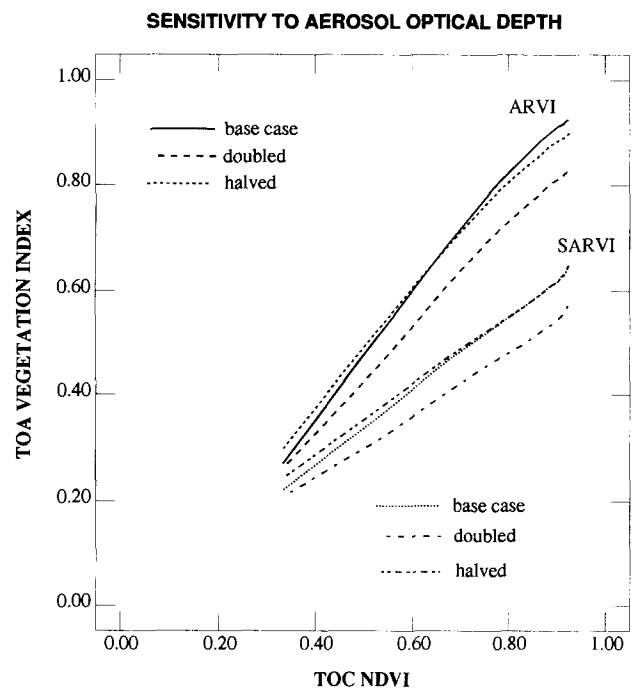


Figure 9b. Influence of aerosol optical depth on the relationship between ARVI and SARVI to top-of-the-canopy NDVI. Aerosol optical depth in the base case problem parameter set was doubled (turbid atmosphere) and halved (clear atmosphere) to effect a sensitivity analysis.

radiative transfer problem. A horizontally homogeneous, cloudless, midlatitude, continental atmosphere with both molecular and aerosol loading is assumed throughout. The canopy and atmospheric radiative transfer equations are numerically solved by the standard discrete ordinates method. A total of 13 discrete wavelengths in the solar spectrum were considered in this study.

Radiance distribution in the principal plane above the canopy and atmosphere differ considerably due to the nature of atmospheric effects that are wavelength-dependent. The net atmospheric effect is positive at shorter wavelengths ( $< 0.7 \mu\text{m}$ ) where scattering in the atmosphere dominates. Conversely, the net atmospheric effect is negative at longer wavelengths ( $> 1.0 \mu\text{m}$ ) where absorption in the atmosphere predominates. The anisotropy of the radiance distribution increases with solar zenith angle.

Top-of-the-canopy (TOC) NDVI angular distribution of dense vegetation canopies shows a minimum value in the retrosolar direction. The hot spot effect in this direction results in a high red canopy reflectance which decreases the contrast (lower NDVI). Also, NDVIs in the backscattering directions are lower than those in the forward scattering directions. Top-of-the-atmosphere (TOA) NDVI is always smaller than TOC NDVI because of a positive net atmospheric effect at the red wavelength. Dense canopy ARVI distribution in the principal plane is similar to TOC NDVI distribution for moderate view angles ( $< 50^\circ$ ), indicating a correction for atmospheric effects.

The relationship between TOA NDVI and TOC NDVI is not influenced by the leaf normal orientation distribution and leaf optical properties in the visible wavelengths. However, this relationship is sensitive to soil reflectance, high solar zenith angle, and aerosol optical depth. Soil brightness effects can be minimized if SAVI is utilized. Both NDVI and SAVI are subject to atmospheric effects. The spectral index ARVI corrects well for atmospheric effects resulting from sun angle changes and moderate variations in aerosol optical depth. However, ARVI does not correct for the net negative atmospheric effect at the near-infrared wavelength, which in most cases is rather small. However, under turbid atmospheres, the residual atmospheric effect at this wavelength can be large enough to warrant a correction. In spite of this caveat, the slope of the relationship between ARVI and TOC NDVI is close to unity and invariant of leaf normal orientation and leaf optical properties at visible wavelengths. Like NDVI, ARVI is subject to soil brightness effects. When ARVI is combined with SAVI to result in SARVI, there is a certain loss of ability to correct for atmospheric effects as compared to ARVI, but soil influences are generally well corrected.

NASA Grant NAS5-30442. We acknowledge discussions with Drs. Tanré and Kaufman.

## REFERENCES

- Ahmad, S., and Deering, D. W. (1992), A simple analytic function for bidirectional reflectance, *J. Geophys. Res.*, forthcoming.
- Asrar, G., Fuchs, M., Kanemasu, E. T., and Hatfield, J. H. (1984), Estimating absorbed photosynthetic radiation and leaf area index from spectral reflectance in wheat, *Agron. J.* 76:300-306.
- Asrar, G., Myneni, R. B., Li, Y., and Kanemasu, E. T. (1989), Measuring and modeling spectral characteristics of a tall-grass prairie, *Remote Sens. Environ.* 27:143-155.
- Choudhury, B. J. (1987), Relationships between vegetation indices, radiation absorption, and net photosynthesis evaluated by a sensitivity analysis, *Remote Sens. Environ.* 22: 209-233.
- Deepak, A., and Gerber, H. E. (Eds.) (1983), *Report of WMO (CAS) / Radiation Commission of IAMAP Meeting of Experts on Aerosols and their Climatic Effects*, Williamsburg, Virginia, 28-30 March, Report No. WCP-55, World Meteorological Organisation, Geneva.
- Deering, D. W. (1989), Field measurements of bidirectional reflectance, in *Theory and Applications of Optical Remote Sensing* (G. Asrar, Ed.), Wiley, New York, pp. 14-61.
- Ganapol, B. D., and Myneni, R. B. (1992), The  $F_n$  method for the one-angle radiative transfer equation applied to plant canopies, *Remote Sens. Environ.* 39:213-231.
- Goward, S. N., and Huemmerich, K. F. (1992), Vegetation canopy PAR absorptance and the normalized difference vegetation index: an assessment using the SAIL model, *Remote Sens. Environ.* 39:119-140.
- Huete, A. R. (1988), A soil-adjusted vegetation index (SAVI), *Remote Sens. Environ.* 25:295-309.
- Irons, J. R., Weismiller, R. A., and Petersen, G. W. (1989), Soil reflectance, in *Theory and Applications of Optical Remote Sensing* (G. Asrar, Ed.), Wiley, New York, pp. 66-101.
- Kaufman, Y. J. (1989), The atmospheric effect on remote sensing and its corrections, in *Theory and Applications of Optical Remote Sensing* (G. Asrar, Ed.), Wiley, New York, pp. 336-428.
- Kaufman, Y. J., and Tanré, D. (1992), Atmospherically resistant vegetation index (ARVI) for EOS-MODIS, *IEEE Trans. Geosci. Remote Sens.* 30:261-270.
- Marshak, A. L. (1989), The effect of the hot spot on the transport equation in plant canopies, *J. Quant. Spectrosc. Radiat. Transfer* 42:615-630.
- Myneni, R. B., Gutschick, V. P., Asrar, G., and Kanemasu, E. T. (1988a), Photon transport in vegetation canopies with anisotropic scattering: Part II. Discrete-ordinates finite-difference exact-kernel technique for photon transport in slab geometry for the one-angle problem, *Agric. For. Meteorol.* 42:17-40.
- Myneni, R. B., Gutschick, V. P., Asrar, G., and Kanemasu, E. T. (1988b), Photon transport in vegetation canopies with anisotropic scattering: Part IV. Discrete-ordinates finite-difference exact-kernel technique for photon transport in slab

- geometry for the two-angle problem. *Agric. For. Meteorol.* 42:101-120.
- Myneni, R. B., Asrar, G., and Gerstl, S. A. W. (1990), Radiative transfer in three dimensional leaf canopies, *Trans. Theory Stat. Phys.* 19:205-250.
- Myneni, R. B., Marshak, A. L., and Knyazikhin, Yu. (1991), Transport theory for leaf canopies with finite dimensional scattering centers, *J. Quant. Spectrosc. Radiat. Transfer* 46: 259-280.
- Myneni, R. B., Asrar, G., and Hall, F. G. (1992a), A three dimensional radiative transfer model for optical remote sensing of vegetated land surfaces, *Remote Sens. Environ.* 41:85-103.
- Myneni, R. B., Asrar, G., Tanré, D., and Choudhury, B. J. (1992b), Remote sensing of solar radiation absorbed and reflected by vegetated land surfaces, *IEEE Trans. Geosci. Remote Sens.* 30:302-314.
- Myneni, R. B., Ganapol, B. D., and Asrar, G. (1992c), Remote sensing of vegetation canopy photosynthetic and stomatal efficiencies, *Remote Sens. Environ.* 42:217-238.
- Myneni, R. B., Impens, I., and Asrar, G. (1992d), Simulation of space measurements of vegetation canopy bidirectional reflectance factors, *Remote Sens. Rev.* 7:19-41.
- Peterson, D. L., and Running, S. T. (1989), Applications in forest science and management, in *Theory and Applications of Optical Remote Sensing* (G. Asrar, Ed.), Wiley, New York, pp. 429-473.
- Prince, S. D. (1991), A model of regional primary production for use with coarse resolution satellite data, *Int. J. Remote Sens.* 12:1313-1330.
- Ross, J. (1981), *The Radiation Regime and Architecture of Plant Stands*, Dr. W. Junk, Den Haag, The Netherlands.
- Sellers, P. (1985), Canopy reflectance, photosynthesis and transpiration, *Int. J. Remote Sens.* 8:1335-1372.
- Sellers, P. J., Mintz, Y., Sud, Y. C., and Dalcher, A. (1986), A simple biosphere model (SiB) for use within general circulation models, *J. Atmos. Sci.* 43:505-531.
- Shettle, E. P., and Fenn, R. W. (1979), Models for the aerosols of the lower atmosphere and the effects of humidity variations on their optical properties, AFGL-TR-79-0214.
- Shultis, J. K., and Myneni, R. B. (1988), Radiative transfer in vegetation canopies with anisotropic scattering, *J. Quant. Spectrosc. Radiat. Transfer* 39:115-129.
- Stewart, R. (1990), Modeling radiant energy transfer in vegetation canopies. M.S. thesis, Kansas State University, Manhattan.
- Stoner, E. R., and Baumgardner, M. F. (1981), Characteristic variations in reflectance of surface soils, *Soil Sci. Soc. Am. J.* 45:1161-1165.
- Tanré, D., Herman, M., and Deschamps, P. Y. (1983), Influence of the atmosphere on space measurements of directional properties, *Appl. Opt.* 22:733-741.
- Tanré, D., Deroo, C., Duhaut, P., et al. (1990), Description of a computer code to simulate the satellite signal in the solar spectrum: the 5S code, *Int. J. Remote Sens.* 11:659-668.
- Tucker, C. J. (1979), Red and photographic infrared linear combinations for monitoring vegetation, *Remote Sens. Environ.* 8:127-150.